Appl Phys B (2011) 102: 443–450
DOI 10.1007/s00340-010-4323-0

Applied Physics B
Lasers and Optics

Spatial light modulators for the manipulation of individual atoms

L. Brandt · C. Muldoon · T. Thiele · J. Dong · E. Brainis · A. Kuhn

Received: 4 August 2010 / Revised version: 25 October 2010 / Published online: 17 December 2010
© Springer-Verlag 2010

Abstract We propose a versatile arrangement for the trapping and manipulation of single atoms in optical tweezers formed by the direct image of a spatial light modulator (SLM). The scheme incorporates a high numerical aperture microscope to map the intensity distribution of a SLM onto a cloud of cold atoms. The regions of high intensity act as optical dipole-force traps. With a SLM fast enough to modify the trapping potential in real time, this technique is well suited for the controlled addressing and manipulation of arbitrarily selected atoms.

1 Motivation

Many proposals for large-scale quantum computing [1] or quantum simulation [2] rely on the ability to deterministically manipulate, address and couple individual components of a quantum network. These challenges can be addressed by the use of isolated quantum systems, such as trapped ions in quantum computing and entanglement experiments [3, 4], or dipole-trapped single neutral atoms [5–7]. In an effective one-dimensional arrangement it has already been shown that addressing and preparation of individual dipole-trapped atoms is possible and that those atoms can also be used as a phase preserving quantum register [8]. To control a larger number of atoms in a two or three-dimensional quantum network, more elaborate techniques are required. Therefore several methods for handling individual atoms have been developed. The most promising techniques are the trapping of ion strings [3, 4, 9], magnetically trapped neutral atoms above atom chips [10–12], individual atoms in steep optical dipole-force traps [6], optical lattices [7], and dipole-trap arrays created either by a matrix of lenses [13], by holograms [14], or by a combination of these techniques [15]. In contrast to these attempts, we propose to use a spatial light modulator (SLM) [16, 17] as an amplitude modulator to form the desired two-dimensional trapping potential, by directly imaging the SLM. This concept has much in common with the optical-tweezer technique used in biology [18], where light is used to manipulate small objects, like viruses, bacteria, or organic samples attached to microspheres. Here we propose to apply this technique directly to individual atoms. This combination of the SLM with optical tweezers offers atom-chip like flexibility of individual-atom manipulation as well as magnetic-field free dipole trapping. Furthermore, with SLM refresh rates far above the loss rate of trapped atoms, such an arrangement might allow for the real-time manipulation of atoms.

L. Brandt · C. Muldoon · T. Thiele · J. Dong · A. Kuhn (✉)
Clarendon Laboratory, University of Oxford, Parks Road, Oxford OX1 3PU, UK
e-mail: a.kuhn1@physics.ox.ac.uk

E. Brainis
Service OPERA (CP 194/5), Université libre de Bruxelles, Avenue F.D. Roosevelt 50, 1050 Brussels, Belgium

Present address:
T. Thiele
ETH Zurich, 8093 Zurich, Switzerland

2 Outline

The heart of our setup is an arbitrary pattern of light formed in the object plane of a microscope by directly imaging a SLM. The intensity distribution forms a dipole-trapping potential that should allow handling of individual atoms. Figure 1 illustrates this approach and shows how one can use the same microscope to observe the atoms. Several types of SLM are available which all have the potential to achieve

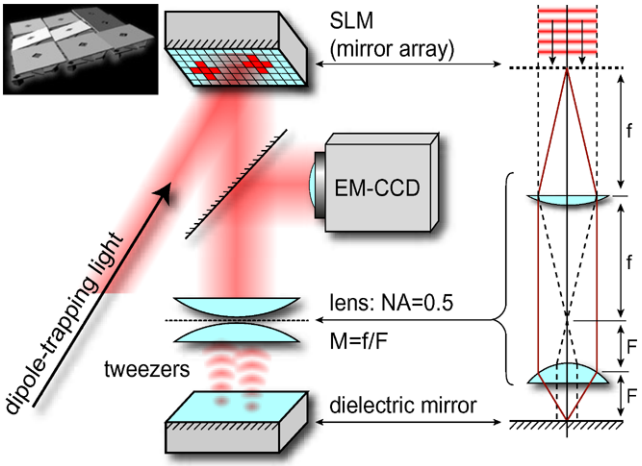

Fig. 1 Scheme of the proposed setup. A *red detuned laser beam* illuminates the mirror array of the SLM. A microscope reproduces the intensity pattern of the SLM near the surface of a mirror placed in the tweezer plane (object plane of the microscope). The reflected light interferes with the incoming beam and forms a standing wave. Its antinodes act as dipole traps, which can hold individual atoms. Since the SLM is reconfigurable, the setup allows arbitrary repositioning of atoms. A very sensitive camera, detecting atomic fluorescence via a dichroic mirror, can be used to observe the trapped atoms and monitor the tweezers in operation. *The insert* (Courtesy of Texas Instruments) shows a block of three by three mirrors of the SLM. The mirrors can be switched between two tilt angles, so that the light is directed either into the microscope or deflected to a beam stop. *On the right hand side*, a possible arrangement of microscope lenses is shown, with SLM and tweezers in conjugate planes for point-to-point imaging from SLM to tweezers (*solid rays*) and isoplanar reproduction of the collimated wave illuminating the SLM in the microscopes object plane [21] (*dashed rays*)

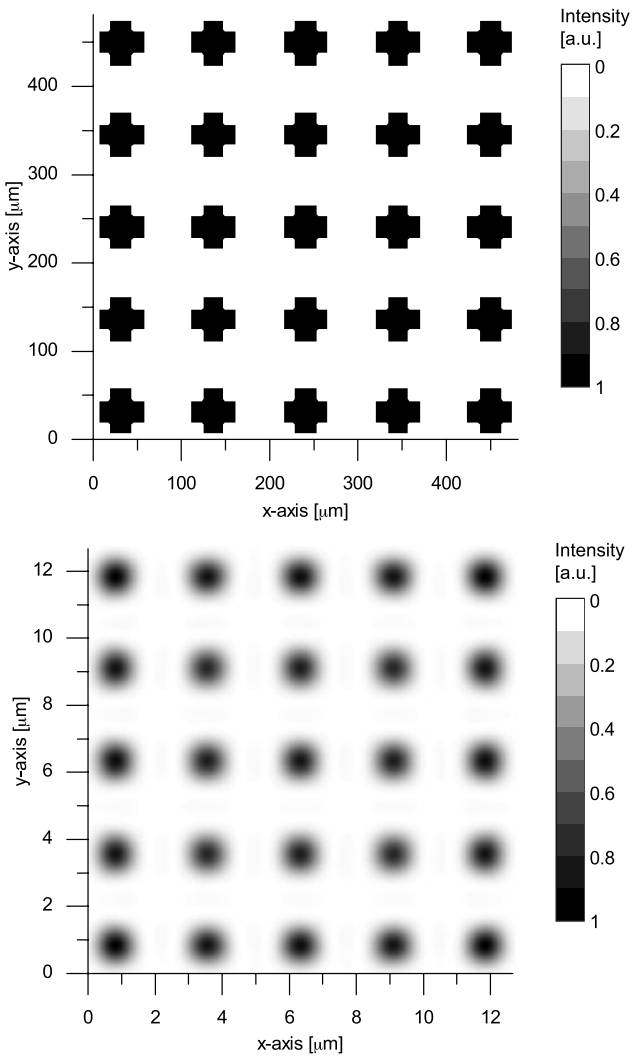

Fig. 2 *The top picture* shows a pattern on the SLM. The pattern is a repetition of a four by four mirror block where the corner pixels are missing. Each mirror has a dimension of 14 μm by 14 μm. *The bottom picture* shows the resulting image when a diffraction-limited lens system with a numerical aperture of $NA = 0.5$ is used to demagnify the pattern by a factor of 1/38. This picture is obtained by convoluting the demagnified pattern from above with airy spots of 1 μm waist

this goal. One widely used technology is the liquid crystal device (LCD) [14, 19]. It has the advantage of creating a range of grey scales, but has the drawback of having a low refresh rate, usually not exceeding 100 Hz. This is in general too slow for the dynamic control of trapped neutral atoms. Other commercially available SLMs are digital mirror devices (DMD) [20]. They consist of an array of individual flat mirrors which can be independently switched between two tilt angles to generate arbitrary intensity distributions. With a full-frame refresh rate of up to 50 kHz and a resolution of typically 1024 by 768 individual mirrors, these devices seem ideal for the real-time manipulation of trapped atoms.

The desired intensity distribution can be formed in two ways. One possibility is to place the SLM in the back focal plane of a lens system, such that its Fourier transform is in the front focal plane. Thus the SLM acts as an effective hologram for the resulting intensity distribution [14]. This method has the drawback that any change in the trapping pattern requires one to recalculate the entire hologram and thus restrains the experimenter to work with predefined sequences. Alternatively, the tweezers can be generated by imaging the surface of an *amplitude-modulating* SLM through a microscope directly onto the atoms. The tweezers are then formed in the object plane of the microscope, see Fig. 2. In the following we concentrate on this latter method, as the direct mapping of intensities provides an intrinsically higher speed and flexibility in the manipulation of trapped atoms. This system can be used to expose the atoms to almost any arbitrarily shaped and time-varying potential landscape, which offers a plethora of applications. Out of these we focus on the implementation of an array of very tiny atom traps, eventually capable of storing single atoms.

The plane of the SLM and the plane where the tweezers are formed are conjugated. Therefore the illumination of the SLM needs to be taken into account. In order to get a uni-

form trap depth for a given pattern like in Fig. 2, the SLM has to be illuminated uniformly. Otherwise the trap depth will vary. Ideally a flat top profile should be used for the illumination. A Gaussian beam could be used as well, provided the beam waist is large enough so that the variation across the SLM stays within bearable limits. If coherent light is used for trapping, a suitable geometry of the illumination has to be chosen to avoid any wavefront-distortion [21].

Any tight spatial confinement of atoms in dipole-force traps relies on small foci of the trapping light. Therefore, an optical system of high numerical aperture is necessary. This can be done with either a sophisticated microscope objective [22] or a single aspheric lens [23]. Typically, these are diffraction limited and have a numerical aperture of 0.5, leading to an optical resolution approximately equal to one wavelength, λ. This also determines the lateral confinement of the atoms. Along the optical axis, the atoms are trapped by the longitudinal beam profile. For a single beam focussed to λ, atoms are axially confined to a Rayleigh length of $\pi \cdot \lambda$. To obtain a better confinement along the optical axis, a standing wave could be used. This can be achieved by placing a mirror at or close to the plane where the tweezers are formed. The atoms trapped in the antinodes of the standing wave are then axially confined to $\lambda/2$.

The underlying physical mechanism used to trap atoms in optical tweezers is the optical dipole force, which atoms experience in detuned light fields. This force is conservative but very weak, resulting in a shallow potential with a typical depth of $\sim$1 mK. Only atoms with low kinetic energy can be trapped, and therefore they need to be pre-cooled before loading them into the tweezers. This is usually accomplished by a magneto-optical trap (MOT), trapping and cooling atoms down to the Doppler cooling limit, $T_D \sim 100$ μK for most alkali atoms [24]. In the case where a mirror is included to form a standing-wave dipole trap, the pre-cooling has to be done close to the mirror surface. This can easily be accomplished using a magneto-optical surface trap (MOST) [25].

3 Feasibility

3.1 Dipole trapping of alkali atoms

The majority of experiments cooling and trapping neutral atoms are done with alkali atoms, of which rubidium is one of the most prominent species. Hence we choose it for the purpose of this feasibility study. The optical tweezers consist of tiny optical dipole-force traps, in which the dynamic Stark shift gives rise to a trapping potential [26]

$$U_{\mathrm{dip}}(\mathbf{r}) \approx \frac{\hbar \Gamma^2}{8\delta} \frac{I(\mathbf{r})}{I_{\mathrm{sat}}} \tag{1}$$

in the *far* detuned limit, where δ is the detuning of the trapping laser light with respect to the atomic transition, $I(\mathbf{r})$ is the intensity of the trapping light, I_{sat} is the saturation intensity for the chosen transition, and Γ is the corresponding decay rate. For red detuned light, $\delta < 0$, U_{dip} is negative and hence attractive. The most critical parameter is the trap depth U_0, which corresponds to the highest intensity of the trapping laser light I_0. Hence U_0 is the energy required for an atom at rest to escape the trap, neglecting gravity. Obviously, the trap depth has to be at least as large as the energy of the pre-cooled atoms. Therefore, the minimum usable trap depth is determined by the temperature that can be reached by the magneto-optical trap. For rubidium, the Doppler cooling limit would be $T_D = 143$ μK. However, it is desirable to operate deeper traps since the spatial confinement of the atoms increases with depth. For atoms whose kinetic energy is smaller than the potential depth by a sufficient amount, the trap can be treated as harmonic, and the spatial confinement of the atoms can be determined by the harmonic oscillation frequencies ω_r and ω_z for radial and longitudinal motion, respectively. The achievable values of U_0, ω_r, and ω_z depend on the wavelength λ of the trapping laser, its intensity, and the trap geometry.

In the proposed scheme (Fig. 1), the trap geometry is essentially determined by the distance L between the focal plane of the optical system which generates the tweezers and the dielectric mirror. The intensity modulation induced by the interference of forward and backward travelling waves over this distance can be seen in Fig. 3. In the following, we first discuss the limiting case $L \to \infty$ (left picture of Fig. 3), which corresponds to having no mirror at all, and then analyse the longitudinal intensity modulation for finite L.

When the dielectric mirror is not present ($L \to \infty$), the trapping potential has a single minimum at the beam waist, in the focal plane of the lens system. The maximum achievable intensity at that point is

$$I_0 = I_d \cdot M^2, \tag{2}$$

where M is the magnification of the microscope (resulting in a demagnification of the DMD by $1/M$) and $I_d = 10\ \mathrm{W/cm^2}$ is the damage threshold of the DMD. To maximise the spatial control of the atoms, the individual traps should be as small as possible. The smallest achievable trap size is limited by the resolution of the optical system (i.e. the Rayleigh criterion) to

$$D_{\mathrm{min}} = 1.22 \cdot \lambda N. \tag{3}$$

Here, λ is the wavelength of the light used, and N is the f-number related to the numerical aperture NA of the optical system by $N \approx \frac{1}{2NA}$. If an aspherical singlet lens is used, the NA can be as high as 0.5. For this value, a resolution limit

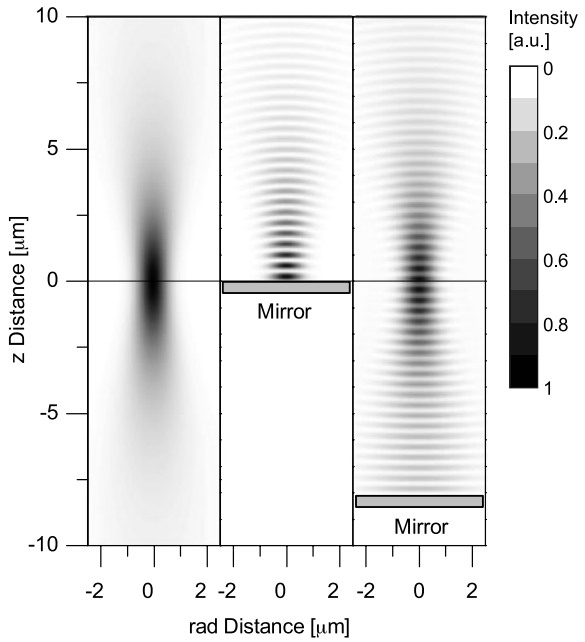

Fig. 3 Intensity distribution of a focused laser beam (with beam waist $w_0 = 0.78$ μm) in the neighbourhood of the focal plane for different distances L between the dielectric mirror and the focal plane. (*Black* corresponds to the highest intensities.) *The left picture* is for $L \to \infty$, i.e. no mirror being present. The tweezer is a pure forward travelling wave with no longitudinal intensity modulation. *The middle picture* shows a beam which is reflected in its focal plane ($L = 0$). The tweezer has a perfect standing-wave pattern, but atoms cannot be trapped in the beam waist. *The right picture* shows the intensity of a retro-reflected beam whose focus lies $L = 8$ μm above the mirror surface. Here the intensity modulation is notably less than in the previous case

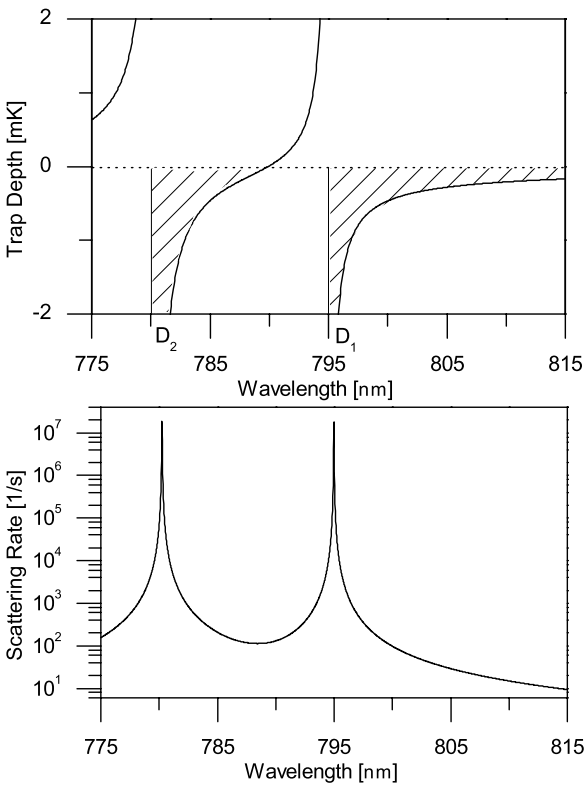

Fig. 4 *The top graph* shows the potential depth of the trap with respect to the wavelength of the trapping light, for linearly polarised light with an intensity of $I_0 = 14.4$ kW/cm^2. The trapping regions are hatched. *The bottom graph* shows the corresponding scattering rate

of $D_{\min} \approx 1$ μm can be reached for $\lambda = 785$ nm, which is well-suited for trapping Rb.

3.2 The role of the SLM

It is important to bear in mind that any experiments involving dynamics require the reconfiguration of the trapping potential. One way atomic transport could be realised is by displacing a pattern of traps. The switching of mirrors would lead to abrupt changes in the trapping potential if the contribution of light for a point in the image plane of the DMD is dominated by one mirror only. If, however, the optical system does not resolve individual mirrors, the reconfiguration of the traps can be smoother, since the light intensity for every point will have contributions from a number of mirrors. Effectively, this leads to grey scales in the trapping pattern. To take advantage of this, we choose the magnification M such that the diagonal of a 2×2 mirror block is not resolved. As the micro-mirrors of a commercially available DMD have a size of 14 μm × 14 μm, a demagnification of $1/38$ is required, i.e. the microscopic magnification should be $M = 38$ (see Fig. 2). According to (2), if the DMD is illuminated with light of an intensity at its damage threshold, an intensity I_0 of 14.4 kW/cm^2 can be obtained at the centre of a tweezer. To ensure a high loading efficiency from the MOT into the tweezers, linear polarised trapping light has to be used [27]. This would saturate the D_2 line of rubidium at an intensity of $I_{\text{sat}} = 2.5$ mW/cm^2. Therefore the maximum intensity is 5.8×10^6 times the saturation intensity. Taking the above discussion into account and requiring a trap depth of 1 mK leads to a detuning $\delta \leq 2.1 \times 10^5 \Gamma$, according to (1). This corresponds to a wavelength detuning of about 2.6 nm to the red with respect to the D_2 line. However, since rubidium has a fine structure splitting of 15 nm, this estimation of the required detuning is certainly too crude. The hyperfine transitions within the D_1 and D_2 lines of Rb need to be taken into account. Two possible wavelength regimes present themselves. The first is slightly red detuned from the D_2 line at 780 nm, and the second is red detuned from the D_1 line at 795 nm (see the top graph of Fig. 4). More specifically, for a trapping laser with an intensity of $I_0 = 14.4$ kW/cm^2, for instance, a trap depth of 1 mK can be achieved for the wavelengths of $\lambda_2 = 782.85$ nm, and $\lambda_1 = 796.90$ nm.

Working with light so close to the D_1 and D_2 resonances gives rise to atomic heating due to photon scattering from the trapping beam. The heating is proportional to the scatter-

ing rate R_{scat}, which, in the far detuned limit [26], is given by

$$R_{\mathrm{scat}} \approx \frac{\Gamma^3}{8\delta^2}\frac{I}{I_{\mathrm{sat}}}. \tag{4}$$

Here we have to take the scattering from both the D_1 and the D_2 line into account, as shown in the bottom graph of Fig. 4. For both λ_1 and λ_2, Rb scatters about 600 photons per second. The scattering rate in both detunings is about the same, since in both cases, the detuning to the closest transition is small when compared to detuning from the other transition. If the trapping laser were further detuned, the region to the red from the D_1 line would be preferable, as the potentials of both lines add constructively there, whereas in the region in-between the D_1 and D_2 lines, the potentials add destructively.

Given that each scattering event involves an exchange of two photons, the kinetic energy of an atom increases on average by twice the recoil energy per scattering event. The lifetime τ of a rubidium atom (initially at rest) in the dipole trap would therefore be limited to $\tau = 1/R_{\mathrm{scat}} \cdot U/2E_{\mathrm{rec}}$. This yields $\tau = 2.3$ s if photon scattering is the only source of heating. It will be shown below that this time is long enough to allow for many transport and detection cycles.

3.3 Radial and axial confinement

We now estimate the radial and longitudinal confinement for a travelling-wave dipole trap ($L \to \infty$). Since a two by two mirror block is spatially not resolved in the object plane of the microscope, we may safely assume that the corresponding intensity distribution is basically limited by diffraction and therefore cylindrically symmetric. The intensity of the light field in the radial direction then reads

$$I(q) = I_0\left(\frac{2\,J_1(q)}{q}\right)^2, \tag{5}$$

where $q = \frac{\pi r}{\lambda N}$, r is the distance from the axis of the trap, and $N \approx 1/(2NA)$ is the f-number, which is about 1 in this case. $J_1(q)$ is a Bessel function of the first kind. For small q, it expands as

$$J_1(q) = \frac{1}{2}q - \frac{1}{16}q^3 + O\left(q^5\right). \tag{6}$$

Inserting this into (5) and keeping only terms up to second order we obtain the harmonic approximation to the trapping potential in the radial direction:

$$U(r) \approx U_0 - \frac{U_0}{4}\left(\frac{\pi}{\lambda N}\right)^2 r^2. \tag{7}$$

Here U_0 is the trap depth, which is plotted in Fig. 4 as a function of the wavelength λ. A particle with mass m oscillates with frequency

$$\omega_r = \sqrt{\frac{-U_0\pi^2}{2m\lambda^2N^2}} \tag{8}$$

in this potential. For $-U_0 = 1\ \mathrm{mK} \cdot k_B$, this leads to a radial trapping frequency of $\omega_r = 2\pi \cdot 162$ kHz. If we approximate this as a Gaussian distribution, the beam waist would be $w_0 = 2\sqrt{2}\lambda N/\pi = 0.71$ µm, which is in agreement with the expected resolution limit. The oscillation frequency along the axial direction ω_z can be calculated using the Rayleigh length $z_0 = \pi\ w_0^2/\lambda \approx 2.0$ µm:

$$\omega_z = \sqrt{\frac{-2U_0}{mz_0^2}}. \tag{9}$$

For $-U_0 = 1\ \mathrm{mK} \cdot k_B$, this yields $\omega_z = 2\pi \cdot 35$ kHz. The axial trapping frequency ω_z is significantly lower than the radial trapping frequency ω_r, which is generally the case for running wave optical dipole-force traps.

We now consider the dielectric mirror to be in the object plane of the microscope $L = 0$. The backward travelling wave interferes with the forward travelling wave and gives rise to a longitudinal interference pattern, creating an ideal standing wave (see the central picture of Fig. 3). The potential has many local minima in which atoms can be trapped. The intensity modulation along the z-axis gives rise to the longitudinal potential

$$U(z) = A(z)\sin^2\left(\frac{2\pi}{\lambda}z\right). \tag{10}$$

The envelope of the modulation, $A(z) = 4U_0/(1 + z^2/z_0^2)$, reaches its maximum at the mirror surface. Here U_0 is the potential depth only due to a single focused beam. Because the contrast of the modulation is one, $A(z)$ is also the trap depth of a local minimum at height z above the mirror. The largest achievable trap depth is $4U_0$, four times higher than without mirror. Therefore the maximum radial trapping frequency in the standing-wave configuration is $\omega_r^{\mathrm{st}} = 2\omega_r = 2\pi \cdot 324$ kHz and is achieved close to the mirror. The longitudinal oscillation frequency inside a local trap at height z is given by

$$\omega_z^{\mathrm{st}}(z) = \sqrt{\frac{-8A(z)\pi^2}{m\lambda^2}}. \tag{11}$$

Close to the mirror, the highest value $\omega_z^{\mathrm{st}} = 2\pi \cdot 1100$ kHz is achieved. Note that, strictly speaking, the first antinode is $\lambda/4$ above the mirror. This slightly reduces the trap depth, but the correction is so small that we may safely neglect it.

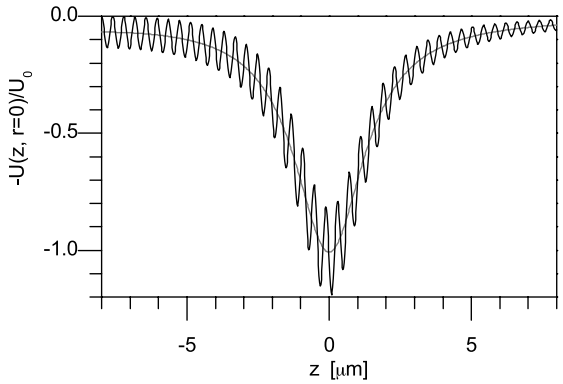

Fig. 5 Potential depth $U(z)$ along the axis, with the focal point 8 μm away from the mirror surface. The slowly varying average of the potential (*grey*) is a feature of focussing the light, whereas the oscillation (*black*) is caused by the partial standing wave. The modulation has the highest visibility close to the mirror surface, becomes less pronounced in the focal spot, and then increases again further away from the focal point

When the mirror is not exactly in the image plane of the DMD (finite distance L), the forwards and backwards propagating waves do not have the same amplitude. Therefore the longitudinal intensity modulation, whose peak-to-peak amplitude is

$$A(z) = \frac{4U_0}{\sqrt{1+z^2/z_0^2}\sqrt{1+(2L+z)^2/z_0^2}}, \tag{12}$$

where the origin for z is defined to be the beam waist and the mirror surface is situated at $z = -L$. The amplitude $A(z)$ rapidly fades away as the distance between the mirror and the focal plane increases. Figure 5 shows the longitudinal potential $U(z)$ for $L = 8$ μm. The deepest local minima are found at the focus of the beam. In general the deepest local minima are at found at $d = \sqrt{L^2 - z_0^2} - L$, for $|L| > |z_0|$, otherwise at $d = -L$, i.e. at the mirror surface. An atom trapped in one of these local minima sees a trap depth of about 1.37 U_0 in the radial direction but only 0.3 U_0 in the longitudinal direction. Whatever the distance between the focal plane and the mirror, the trap depth in the radial direction will always be larger than in the travelling-wave case ($L \to \infty$) but smaller than in the standing-wave case ($L = 0$): 162 kHz $< \omega_r/(2\pi) <$ 324 kHz. Along the z-axis, the trapped atoms are confined either to the slowly varying envelope or to the local minimum, depending on their initial kinetic energy. Only the coldest atoms can be trapped in the local minima. If they are, their confinement shall be strongly improved. In that case the longitudinal frequency can be estimated from (11), with $A(z)$ given by (12). For the example of Fig. 5, one finds that the oscillation frequency at the focus of the beam is $\omega_z = 2\pi \cdot 300$ kHz. Depending on L, the values of ω_z are intermediate between the travelling-wave case ($L \to \infty$) and standing-wave ($L = 0$) case: 35 kHz $< \omega_z/(2\pi) <$ 1100 kHz.

4 Ways to single atoms

In addition to controlling the size and depth of the traps, it is also important to control and measure the number of atoms. More specifically for the goal of conducting single-atom experiments an efficient scheme to prepare single trapped atoms is essential. When loading atoms into moderately sized traps, the number of atoms therein is generally Poisson distributed. In this case, we would need to measure the atom number and then post-select traps with just one atom. Fortunately, for tightly focused dipole traps, the collisional blockade mechanism [28] should give rise to a significant departure from the Poissonian statistics and favour the loading of only one atom per trap.

The effect occurs when atoms are loaded at a rate R from a magneto-optical trap into tightly confined dipole traps. It relies on light-assisted collisions [27] between atoms in the presence of the MOT cooling beam. Provided the latter is strong enough to saturate the transition, two-body losses occur at a rate $\beta' N(N-1)$. N is the atom number and β' is the rate constant, which is inversely proportional to the trapping volume. There is also a single body loss process γN, which is mostly due to background collisions, so the full rate-equation [29] for the entire loading process reads

$$\frac{dN}{dt} = R - \gamma N - \beta' N(N-1). \tag{13}$$

Collisional blockade will occur when the two-body loss rate dominates over the loading rate of the dipole trap. Hence, it will work very efficiently when β' is large, i.e. if the atoms are confined to a tiny volume. The volume occupied by the atoms depends on the temperature and the trapping frequency. A comparison of the frequencies achievable with the proposed set up, and the trapping frequency $\omega_t = 2\pi \cdot 200$ kHz of a previous experiment demonstrating the collisional blockade [28] leads us to the conclusion that here this mechanism could be highly efficient as well. Due to the nature of the collisional blockade, the traps would be filled with a random pattern of atoms, with a filling factor of at most 50%. Nonetheless, in connection with an in-situ atom detection and subsequent rearrangement of occupied traps, scaling to very large arrays of single trapped atoms seems feasible.

5 Single-atom detection and transport

To investigate the loading processes, the atom numbers in the individual traps have to be determined. For well-isolated

traps, laser induced resonance fluorescence could be used for atom counting [30]. To collect the fluorescence, we suggest using the lens system which creates the optical tweezers in backward direction as a microscope, such that a spatially resolved fluorescence image can be obtained by a highly sensitive EM-CCD camera. This technique is well established and nowadays routinely used in many experiments for observing single atoms that are trapped in microscopic dipole traps [31–33].

To discuss the feasibility of single-atom detection, the flux of photons impinging on the camera has to be determined. The geometrical collection efficiency η depends on the numerical aperture of the lens system. To evaluate η, we assume a uniform photon emission of the atoms and calculate the ratio of photons passing through the system. The ratio of the surface area of a spherical cap with that of a sphere, yields $\eta = 2\pi(1-\cos(\frac{\alpha}{2}))/(4\pi)$, where α is the opening angle. For a numerical aperture of 0.5, $\alpha = 60°$, we expect a collection efficiency of $\eta = 0.067$.

If the radiative transition of the atom is completely saturated, the scattering rate on resonance tends to $R_{\mathrm{scat}} = \frac{1}{2}\Gamma$, hence $R_{\mathrm{scat}} = 19.6\ \mu\mathrm{s}^{-1}$ for rubidium. Assuming a further loss of 50% to take the optical system and the limited quantum efficiency of the camera into account, a camera should collect photons from a single atom with a rate of $R_{\mathrm{cam}} = 653\ \mathrm{ms}^{-1}$. In other words, a camera operating with an exposure time of 100 µs could count as many as 65 photons. For modern electron multiplying charged coupled device (EM-CCD) cameras, this is well above the signal to noise threshold, so it is possible to use such devices to observe single atoms. We emphasise that this estimate assumes no direct scattering of probe photons off the dielectric mirror into the camera. The latter effect can be eliminated altogether using probe beams travelling parallel to the mirror surface at a sufficient distance. Moreover, in case these beams are counter-propagating and red detuned, the trapped atoms would be subject to molasses cooling during observation, which allows for long observation times. In particular, this way of monitoring dipole-trapped atoms is not subject to broadening effects that otherwise limit the observation time of atoms in free flight [34–36].

The high frame rate of the DMD should allow for the reconfiguration of the potential landscape, and hence for the transport of confined atoms. A naive method would be to transport atoms adiabatically by changing the potential slowly enough so that the atoms are following without being heated. Since the DMD has only a finite resolution, this must be done using discrete steps. With the aforementioned trap consisting of a four by four block, as shown in Fig. 2, the pattern would have to be shifted by at most one pixel per step. The longest distance the traps could be moved is 1000 pixels, that is, from one edge of the DMD to the other. With a refresh rate of 50 kHz, this transport would take 20 ms. This is much shorter than the anticipated lifetime of the trap, which should be of at least several 100 ms. However a drawback of this method is that discrete switching of mirror elements leads to parametric heating of the atoms. To circumvent this, the atom-transport could also be realised ballistically. The initially trapped atoms would be accelerated through a sudden change in trapping potential, guided through a channel and eventually decelerated and recaptured. This scheme has the advantage that it needs only a few changes in the potential, making it less susceptible to heating, and yet faster at the same time.

6 Conclusion and outlook

Our study shows that the handling and manipulation of individual dipole-trapped atoms should be possible with a two-dimensional optical-tweezer type setup with the technologies at our disposal today. Using this new scheme, real-time arrangement of dipole traps is possible, and two-dimensional transport of single atoms seems feasible. We expect this technique to boost the field of quantum computing, as it will allow one to handle single entities within a large scalable array. For instance, pairwise entanglement could be achieved through either cavity QED [37], as one could place a fibre-tip micro cavity [38] around the trapping region, or with controlled collisions [39], which one could implement through a spin-selective trapping scheme [5]. This would then allow for generating large cluster states which are the essential resource for one-way quantum computing [40]. We also note that the proposed scheme can be extended to three dimensions, using either a second setup of the same kind perpendicular to the first, or with additional light sheets running perpendicular to the optical axis to select individual trapping planes within the standing-wave geometry.

Acknowledgements We thank Matthew Himsworth for helpful discussions. This work was supported by the Engineering and Physical Sciences Research Council (EP/ E023568/1), the Deutsche Forschungsgemeinschaft (Research Unit 635), the Belgian Fonds de la Recherche Scientifique—FNRS, the Philippe Wiener and Maurice Anspach Foundation, and the EU through the RTN EMALI (MRTN-CT-2006-035369) and the IST programme SCALA.

References

1. D.P. DiVincenzo, Fortschr. Phys. **48**, 771 (2000)
2. I. Buluta, F. Nori, Science **326**, 108 (2009)
3. H. Häffner, C.F. Roos, R. Blatt, Phys. Rep. **469**, 155 (2008)
4. R. Blatt, D.J. Wineland, Nature **453**, 1008 (2008)
5. M. Karski, L. Förster, J. Choi, A. Steffen, W. Alt, D. Meschede, A. Widera, Science **325**, 174 (2009)
6. J. Beugnon, C. Tuchendler, H. Marion, A. Gaëtan, Y. Miroshnychenko, Y.R.P. Sortais, A.M. Lance, M.P.A. Jones, G. Messin, A. Browaeys, P. Grangier, Nat. Phys. **3**, 696 (2007)

7. I. Bloch, Nature **453**, 1016 (2008)
8. D. Schrader, I. Dotsenko, M. Khudaverdyan, Y. Miroshnychenko, A. Rauschenbeutel, D. Meschede, Phys. Rev. Lett. **93**, 150501 (2004)
9. M. Riebe, T. Monz, A.S. Villar, P. Schindler, M. Chwalla, M. Hennrich, R. Blatt, Nat. Phys. **4**, 839 (2008)
10. R.J. Sewell, J. Dingjan, F. Baumgärtner, I. Llorente-García, S. Eriksson, E.A. Hinds, G. Lewis, P. Srinivasan, Z. Moktadir, C.O. Gollasch, M. Kraft, J. Phys. B, At. Mol. Opt. Phys. **43**, 051003 (2010)
11. D. Heine, M. Wilzbach, T. Raub, B. Hessmo, J. Schmiedmayer, Phys. Rev. A **79**, 021804(R) (2009)
12. W. Hänsel, P. Hommelhoff, T.W. Hänsch, J. Reichel, Nature **413**, 498 (2001)
13. A. Lengwenus, J. Kruse, M. Schlosser, S. Tichelmann, G. Birkl, Phys. Rev. Lett. **105**, 170502 (2010)
14. S. Bergamini, B. Darquié, M. Jones, L. Jacubowiez, A. Browaeys, P. Grangier, J. Opt. Soc. Am. B **21**, 1889 (2004)
15. W.S. Bakr, J.I. Gillen, A. Peng, S. Foelling, M. Greiner, Nature **462**, 74 (2009)
16. C. MacAulay, A. Dlugan, Proc. SPIE **3260**, 201 (1998)
17. Q.S. Hanley, P.J. Verveer, M.J. Gemkow, D. Arndt-Jovin, T.M. Jovin, J. Microsc. **196**, 317 (1999)
18. A. Ashkin, J.M. Dziedzic, Science **235**, 1517 (1987)
19. J. Kruse, C. Gierl, M. Schlosser, G. Birkl, Phys. Rev. A **81**, 060308(R) (2010)
20. P.F. Van Kessel, L.J. Hornbeck, R.E. Meier, M.R. Douglass, Proc. IEEE **86**, 1687 (1998)
21. E. Brainis, C. Muldoon, L. Brandt, A. Kuhn, Opt. Commun. **282**, 465 (2009)
22. W. Alt, Int. J. Light Electron Opt. **113**, 142 (2002)
23. Y.R.P. Sortais, H. Marion, C. Tuchendler, A.M. Lance, M. Lamare, P. Fournet, C. Armellin, R. Mercier, G. Messin, A. Browaeys, P. Grangier, Phys. Rev. A **75**, 013406 (2007)
24. H.J. Metcalf, P. van der Straten, *Laser Cooling and Trapping* (Springer, New York, 1999)
25. S. Wildermuth, P. Krüger, C. Becker, M. Brajdic, S. Haupt, A. Kasper, R. Folman, J. Schmiedmayer, Phys. Rev. A **69**, 030901 (2004)
26. C.J. Foot, *Atomic Physics* (Oxford University Press, Oxford, 2005)
27. S.J.M. Kuppens, K.L. Corwin, K.W. Miller, T.E. Chupp, C.E. Wieman, Phys. Rev. A **62**, 013406 (2000)
28. N. Schlosser, G. Reymond, I. Protsenko, P. Grangier, Nature **411**, 1024 (2001)
29. N. Schlosser, G. Reymond, P. Grangier, Phys. Rev. Lett. **89**, 023005 (2002)
30. D. Frese, B. Ueberholz, S. Kuhr, W. Alt, D. Schrader, V. Gomer, D. Meschede, Phys. Rev. Lett. **85**, 3777 (2000)
31. J. Beugnon, C. Tuchendler, H. Marion, A. Gaëtan, Y. Miroshnychenko, Y.R.P. Sortais, A.M. Lance, M.P.A. Jones, G. Messin, A. Browaeys, P. Grangier, Nat. Phys. **3**, 696 (2007)
32. I. Dotsenko, W. Alt, M. Khudaverdyan, S. Kuhr, D. Meschede, Y. Miroshnychenko, D. Schrader, A. Rauschenbeutel, Phys. Rev. Lett. **95**, 033002 (2005)
33. M. Mücke, E. Figueroa, J. Bochmann, C. Hahn, K. Murr, S. Ritter, C.J. Villas-Boas, G. Rempe, Nature **465**, 755(2010)
34. T. Bondo, M. Hennrich, T. Legero, G. Rempe, A. Kuhn, Opt. Commun. **264**, 271(2006)
35. A. Fuhrmanek, A.M. Lance, C. Tuchendler, P. Grangier, Y.R.P. Sortais, A. Browaeys, New J. Phys. **12**, 053028 (2010)
36. A. Fuhrmanek, Y.R.P. Sortais, P. Grangier, A. Browaeys, Phys. Rev. A **82**, 023623 (2010)
37. T. Pellizzari, Phys. Rev. Lett. **79**, 5242 (1997)
38. T. Steinmetz, Y. Colombe, D. Hunger, T.W. Hänsch, A. Balocchi, R.J. Warburton, J. Reichel, Appl. Phys. Lett. **89**, 111110 (2006)
39. D. Jaksch, H.-J. Briegel, J.I. Cirac, C.W. Gardiner, P. Zoller, Phys. Rev. Lett. **82**, 1975 (1999)
40. R. Raussendorf, H.J. Briegel, Phys. Rev. Lett. **86**, 5188 (2001)